Effects of graphene content on the microstructure and properties of copper matrix composites

Fanyan Chen [a], Jiamin Ying [a], Yifei Wang [a], Shiyu Du [a], Zhaoping Liu [b], Qing Huang [a, *]

[a] *Engineering Laboratory of Specialty Fibers and Nuclear Energy Materials, Ningbo Institute of Industrial Technology, Chinese Academy of Sciences, Ningbo, Zhejiang 315201, China*

[b] *Advanced Lithium Ions Batteries Engineering Laboratory, Ningbo Institute of Industrial Technology, Chinese Academy of Sciences, Ningbo, Zhejiang 315201, China*

ARTICLE INFO

ABSTRACT

Copper matrix composites reinforced with graphene nanoplatelets (GNPs) were prepared via molecular-level mixing process and spark plasma sintering process. The impacts of graphene content on microstructure, mechanical performance, thermal diffusivity, electrical conductivity and tribological properties of the composites were investigated. For microstructure, GNPs distributed randomly in composites with low graphene concentration (no more than 0.8 vol.%), but aligned in the direction perpendicular to the consolidation force when graphene concentration was above 2.0 vol.%. The mechanical performance of copper was strengthened evidently by the graphene addition. However, the strengthen effects were firstly enhanced and then deteriorated by increasing graphene content. Thermal diffusivity showed a constant decrease with the increase of graphene content. Anisotropy thermal performance was obtained by composites with graphene alignment. Furthermore, graphene addition showed little negative impact on electrical conductivity but dramatically improved tribological performance.

1. Introduction

Graphene, a newly emerged carbon material, has gained considerable attention owing to its extraordinary mechanical, thermal and electrical properties [1]. Compared with carbon-nanotubes (CNTs), graphene possesses 2D sheet-like structure with larger surface area and much lower production cost, which makes it a good alternative strengthening material for composites [2]. In fact, Koratkar's research had confirmed the better strengthening effect of graphene than CNTs in mechanical performance of epoxy composite [3]. In recent years, graphene has become a popular nanofiller material for polymer matrix composites [4–6]. However, the reported metal matrix graphene composites are in limited kinds [7–10].

Copper/graphene composite is one of the few studied metal matrix composites strengthened by graphene. Introducing graphene into copper matrix is hoping to further improve the mechanical, electrical and thermal performance. However, driven by the van der Waals forces, graphene nanoplatelets (GNPs) are prone to agglomerate during fabrication process. In addition, effective interface bonding cannot be obtained due to the poor affinity of graphene to copper. Thus, to fabricate high performance copper/graphene composites needs to meet two main requirements: i) uniform dispersion of graphene in the matrix and ii) sufficient interface strength between copper and graphene. As agglomeration and structural destruction of carbon filler often take place during ball-milling process of conventional powder metallurgy method [11,12], novel or modified fabrication methods were employed to fabricate copper/graphene composites. Hwang et al dispersed RGO uniformly into copper matrix and obtained significantly improved mechanical performance by molecular-level mixing method [13]. Li et al found decorating graphene flakes with Ni nanoparticles not only prevented agglomeration but also improved bonding strength between graphene and copper matrix [14]. Strengthened copper/graphene composites have also been obtained by several other methods, such as electrodeposition [15], high-ratio differential speed rooling [16] and layer by layer method [17], etc. However, as all these research work were focusing on discussing the effectiveness of fabrication method, the impacts of graphene content on the properties of copper/graphene composites were seldom studied, even when composites with varied graphene contents were

* Corresponding author.
E-mail address: huangqing@nimte.ac.cn (Q. Huang).

prepared in some work [13,16]. For conventional powder metallurgy method, Chu's work discussed the mechanical performance of copper matrix composites with graphene in a wide content range [18]. However, as graphene agglomerates were formed in composites with high graphene content, the performance was affected by graphene agglomerations.

In this study, in order to reflect the impacts of graphene concentration on composite properties without the influence of graphene agglomeration, copper matrix composites with varied graphene contents (Cu/GNPs) were prepared via molecular-level mixing process and spark plasma sintering (SPS) process. The effects of graphene content on the microstructure, mechanical properties, thermal diffusivity, electrical conductivity and tribological performance of the composites were thoroughly investigated. More importantly, the mechanisms of the effects were analyzed in detail.

2. Experimental

2.1. Fabrication of Cu/GNPs composite powders

The GNPs were provided by Ningbo Morsh Technology. Co. Ltd. in the form of graphene paste. The graphene platelets were about 2.4 nm in thickness, ranging from 5 to 15 μm. The chemicals used were all purchased from Aladdin Industrial Corporation at analytical grade. Cu/GNPs composite powders were fabricated by a molecular-level mixing process which involved: 1) suspending graphene in the alcoholic solution of Cu ion, 2) reducing Cu ion to form Cu_2O/graphene composite precipitate using $C_6H_{12}O_6$, 3) washing and drying the Cu_2O/GNPs composite powders and 4) reducing Cu_2O to Cu in H_2 atmosphere. Detail fabrication process was as follows: A certain amount of GNPs was dispersed into 1000 ml alcoholic solution of $Cu(NO_3)_2 \cdot 3H_2O$ (96.64 g) by sonicating for 1 h. 100 ml 2 M aqueous solution of $C_6H_{12}O_6$ was then mixed with the graphene solution by further sonication. After that, 500 ml 2 M NaOH aqueous solution was slowly added into the mixed solution with constant stirring. The obtained solution was then kept in an oven at 80 °C for 4 h. The precipitated Cu_2O/GNPs powders were filtered and washed with 50 vol.% ethanol solution before being dried at 60 °C under vacuum. After that, the powders were reduced in H_2 atmosphere at 300 °C for 3 h to obtain Cu/GNPs composite powders. By adjusting the amount of GNPs, composite powders with 0.2 vol.%, 0.4 vol.%, 0.6 vol.%, 0.8 vol.%, 2.0 vol.% and 4.0 vol.% graphene were fabricated. The adopted density of graphene was 2.2 g/cm^3.

2.2. Fabrication of bulk Cu/GNPs composites

The as-prepared Cu/GNPs composite powders with varied graphene contents were sintered into discs with 20 mm in diameter by spark plasma sintering (SPS) at 700 °C for 5 min under vacuum. The corresponding bulk Cu/GNPs composites were denoted as Cu-0.2 vol.% GNPs, Cu-0.4 vol.% GNPs, Cu-0.6 vol.% GNPs, Cu-0.8 vol.% GNPs, Cu-2.0 vol.% GNPs and Cu-4.0 vol.% GNPs, respectively. A consolidation pressure of 40 MPa was applied and held from the beginning until a larger pressure of 50 MPa was applied during the whole cooling process.

2.3. Characterizations

The microstructures of the composite powders and bulk composites were examined by a field emission scanning microscopy (SEM) (FEI Quanta FEG 250). X-ray diffraction (XRD) analysis for the composite powders was performed on a Bruker D8 ADVANCE X-ray diffractometer using Cu Kα radiation at a scan rate of 2°/min. The presence of graphene in the powders and bulk composites was confirmed by Raman spectroscopy (Renishaw inVia Reflex) using an excitation wavelength of 514 nm. Tensile tests were performed on the universal material tester (Instron 5569A). Elastic modulus and hardness were obtained by nanoindentation (MTS, NANO G200). Light flash method was employed to measure thermal diffusivity with Netzsch LFA 457 MicroFlash. The electrical conductivity was investigated by eddy current method using eddy current conductivity meter (FIRST, FD-120).

To investigate the tribological performance in air, friction tests were conducted on the UMT-3 ball-on-disk multifunctional high temperature tribometer. The disk, made from the as-prepared composites, was kept stationary. A 3 mm Si_3N_4 ball (16 GPa, Ra of 0.01 μm) was chosen as the counterface ball which was in reciprocation motion with 5 mm stroke distance. The sliding speed was set at 0.01 m/s during the friction test. The applied load and duration time were fixed at 5 N and 30 min, respectively. To analyze the wear mechanisms, compositions and morphologies on the wear tracks were examined by Raman spectroscopy, SEM, energy-dispersive X-ray spectroscopy (EDS) and Surface Profiler (Alpha-Step IQ).

3. Results and discussion

3.1. Microstructure of the composite powders and bulk composites

Fig. 1a displays the distribution of graphene in the Cu_2O/GNPs composite powders. All the GNPs are unfolded and distributed homogeneously between Cu_2O nanoparticles. After reduction in H_2 atmosphere, Cu_2O was reduced to Cu and Cu-Graphene-Cu sandwich structure was formed between copper nanoparticles. Both sides of the Graphene plate were covered by copper nanoparticles (Fig. 1b), which effectively prevented the aggregation of the GNPs. The chemical structures of the composite powders are confirmed by XRD analysis shown in Fig. 1d.

By spark plasma sintering, the Cu/GNPs composite powders were sintered into bulk Cu/GNPs composites shown in Fig. 1c. Raman spectroscopy presented in Fig. 1e proves the presence of graphene in the composite powders and bulk composite. The D peak at 1350 cm^{-1} indicates the disorder of carbon material, and its intensity ratio to the G peak at 1580 cm^{-1} (I_D/I_G) is a measure of defects in graphene [19]. And as the intensity ratio of 2D peak (~2725 cm^{-1}) to the G peak (I_{2D}/I_G) is in inverse proportion to the number of graphene layer [20], variation of I_{2D}/I_G can be used to assist analyzing the dispersion of graphene. It is found that both I_D/I_G and I_{2D}/I_G did not change evidently after powder preparation and sintering, which indicates that the composite fabrication process did not increase the defects of the graphene and there were no graphene agglomerations formed in copper matrix.

Fig. 2 shows the fracture surfaces of pure copper and Cu/GNPs composites. It confirms that GNPs were dispersed homogeneously in copper matrix, even when graphene fraction achieved to 4.0 vol.%. The uniform dispersion of GNPs effectively prevented the negative influence of graphene agglomerations on the properties of Cu/GNPs composites. The fracture morphology of pure copper in Fig. 2a exhibits a dimple pattern which is the typical feature of plastic fracture. As the graphene content increases, both the size and depth of the dimples keep decreasing (white circled areas), which is a sign of toughness deterioration of the composites. Some GNPs are exposed entirely on the fracture surface (black circled areas in Fig. 2b and c), which was attributed to the extension of cracks along the phase interface after interface debonding occurred during fracture process. The fracture surfaces of Cu-2.0 vol.% GNPs (Fig. 2d) and Cu-4.0 vol.% GNPs (Fig. 2e) show the typical character of brittle fracture with no apparent dimple and tear ridge structures

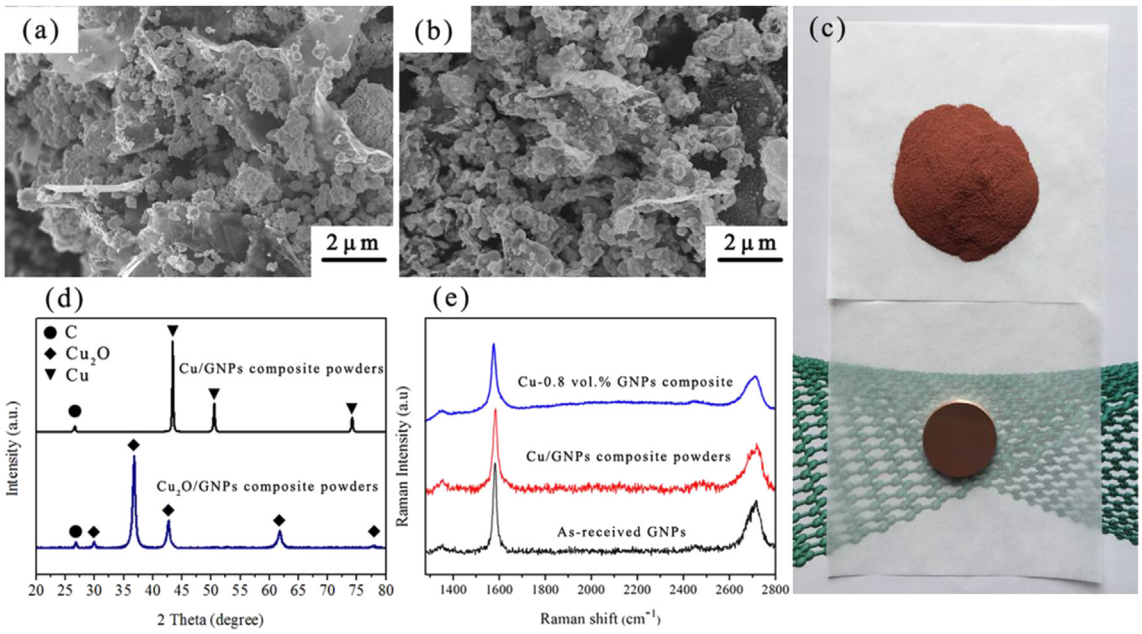

Fig. 1. SEM image of (a) Cu_2O/GNPs, (b) Cu/GNPs, (c) Optical images of Cu/GNPs composite powders and bulk Cu/GNPs composites, (d) XRD results for composite powders and (e) Raman spectroscopy of composite powders and bulk composite. (A colour version of this figure can be viewed online.)

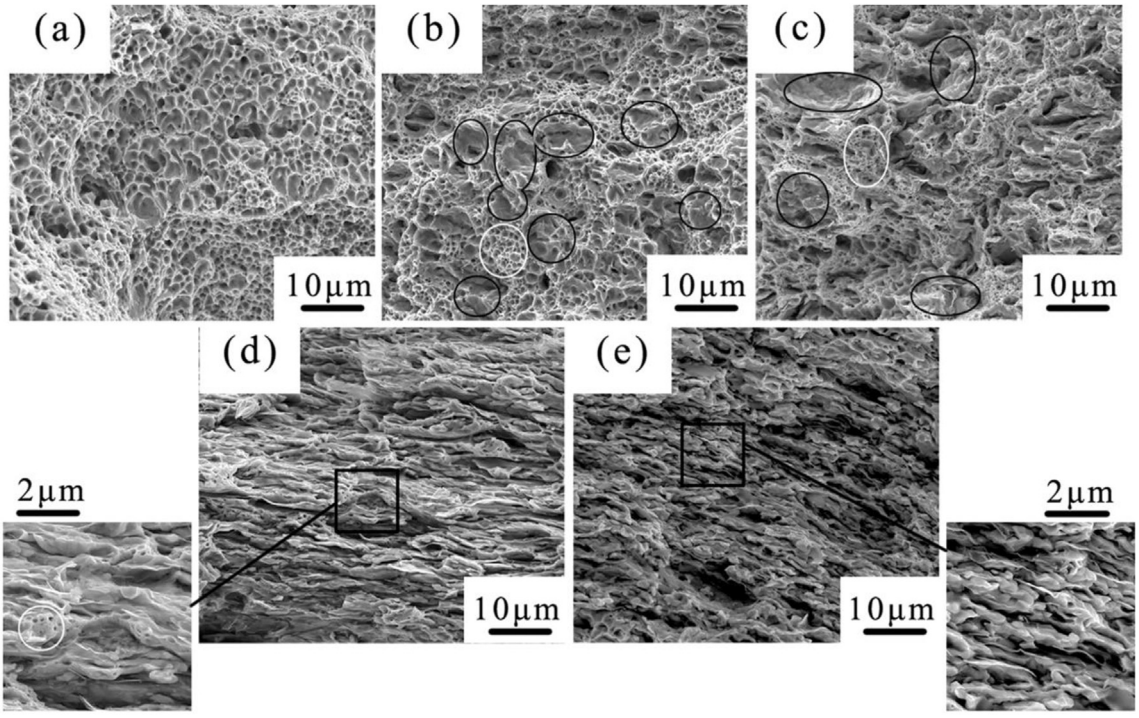

Fig. 2. SEM images for the fracture surface of pure copper and Cu/GNPs composites: (a) pure copper, (b) Cu-0.2 vol.% GNPs, (c) Cu-0.8 vol.% GNPs, (d) Cu-2.0 vol.% GNPs and (e) Cu-4.0 vol.% GNPs.

observed. As the volume fraction of matrix was largely decreased, the copper matrix between GNPs became thin-layer structure and even particle-like structure, as indicated by the magnified views. As a result, the bonding and load transfer effect between the matrix and graphene were weakened, leading to the deterioration of mechanical performance of composites.

Another interesting phenomenon found from Fig. 2 is that the distribution of graphene in the composites was affected by its concentration. When the graphene concentration was no more than 0.8 vol.%, the GNPs distributed randomly. However, for the composites with 2.0 vol.% and 4.0 vol.%, GNPs were aligned in the direction perpendicular to the consolidation force during SPS process. According to the previous study [21], larger size of graphite platelets are more easily to achieve alignment. With high graphene

content, GNPs are more likely to overlap with each other to increase the graphene size, which results in the alignment of graphene.

3.2. Mechanical properties of Cu/GNPs composites

Fig. 3a presents the typical stress–strain curves for the Cu/GNPs composites. For comparison, the stress–strain curve of pure copper prepared by the same process was also tested. Specifically, the fracture mode of the composites with graphene content no more than 0.8 vol.% was plastic fracture, just as pure copper. However, once the filler content increased to 2.0 vol.%, there is no obvious necking stage observed from the stress–strain curve, which means the fracture mode changed from plastic fracture to brittle fracture. This is consistent with the fracture surface analysis for Fig. 2. In order to analyze the variation tendency, the yield strength and fracture elongation as functions of graphene content are summarized in Fig. 3b. For pure copper, the average yield strength is 142 MPa and fracture elongation is about 30%. With the increase of graphene content, the fracture elongation decreases constantly from 30% to 3.5%. In contrast, the yield strength first increases to 310 MPa at the graphene content of 0.6 vol.% and then drops to 200 MPa when the graphene content further increases to 4.0 vol.%. Similarly, both the elastic modulus and hardness of the composites increase to their maximum values before decrease beginning at the graphene content around 0.8 vol.% in Fig. 3c. The highest elastic modulus and hardness obtained were 147 GPa and 1.75 GPa, the increment compared with pure Cu (E ≈ 89 GPa, H ≈ 1.01 GPa) being 65% and 75%, respectively.

Copper was strengthened by graphene through several mechanisms. Graphene addition caused microstructural changes of the metal matrix. One change was a plastic zone with a high dislocation density was generated in the vicinity of the GNPs due to the large thermal expansion mismatch between GNPs and copper matrix [22]. Another important change was an evident decrease in grain size (Fig. S1 in supporting information). Grain size refinement results in increased grain boundary, which increases the resistance to the dislocation movement. The poor affinity between copper and carbon usually causes interface dewetting in composites. However, according to the previous researches, Cu–O bonding forms at the interface of copper matrix composites during molecular mixing process as there are functional groups on the carbon fillers [13,23], which is beneficial to the load transfer between matrix and filler. Since the raw material used in the present work was graphene flakes instead of graphene oxide which has much more defects and functional groups on the lattice, the enhanced effect on the interfacial adherence was unobvious. However, the load transfer between matrix and graphene still could take place due to mechanical interlock effect. The Orowan strengthening is another commonly acknowledged strengthening mechanism in metal matrix composites. However, considering the size and volume fraction of GNPs, the contribution of Orowan strengthening can be safely ignored at the present work [24].

Based on the above discussion, for Cu/GNPs composites, the strengthening effects were considered as deriving from high generated dislocation density, grain size refinement and load transfer effects. In this case, the theoretical model proposed by Y. Wu et al can be used to qualitatively predict the mechanical strength of composites [25]:

$$\sigma_{MMC} = \left[\sigma_{mu}\cdot s/4 + \Delta\sigma_{dis}\cdot\left(s + 4R^2\right)\Big/4 + \Delta\sigma_{SG}\right]\cdot V_f + \sigma_{mu} + \Delta\sigma_{SG} - \Delta\sigma_{int} \quad (1)$$

where σ_{MMC}, σ_{mu}, $\Delta\sigma_{dis}$, $\Delta\sigma_{SG}$ and $\Delta\sigma_{int}$ are the strength of the composite, strength of the unreinforced matrix, the dislocation induced strength increment, the strength increment due to grain size refinement and the internal stress, respectively; s, R and V_f are the aspect ratio, the ratio of the size of the plastic zone to the reinforcement particulate and the volume fraction of the reinforcement, respectively. Due to the scarce research work on microstructure of metal matrix composite with graphene, the accurate strength calculation for Cu/GNPs composites using Wu's model is lack of the required data. However, this model predicts that the strength of the composite is in direct proportion to the volume fraction of reinforcement particulate, which is in conflict with the present experiment results. In fact, this model was founded on the assumption that the reinforcement matrix interface was sufficiently strong to resist debonding during loading. However, interface debonding took place in the composites during tensile tests, as Fig. S2 (supporting information) clearly reveals the pull-out phenomenon of graphene.

The change of fracture mode with increasing graphene concentration was caused by the variation of graphene distribution. With randomly distributed graphene, the generated dislocations at the vicinity of graphene tangled together to form 3D network, which increased the resistance to dislocation movement. Once micro cracks formed, the extension of crack tip was hindered by the high stress distinct localized perpendicular to its direction. The improved resistance to dislocation movement and crack extension enhanced the strengthening and toughening effect of graphene. In contrast, for the composites with graphene alignment, the tensile force was along the shear force direction of the interface, which increased the debonding speed and resulted in the fast failure of material.

3.3. Thermal and electrical performance of Cu/GNPs composites

Since the distribution of graphene was affected by graphene content, the thermal diffusivity parallel ($\alpha_{vertical}$) and perpendicular

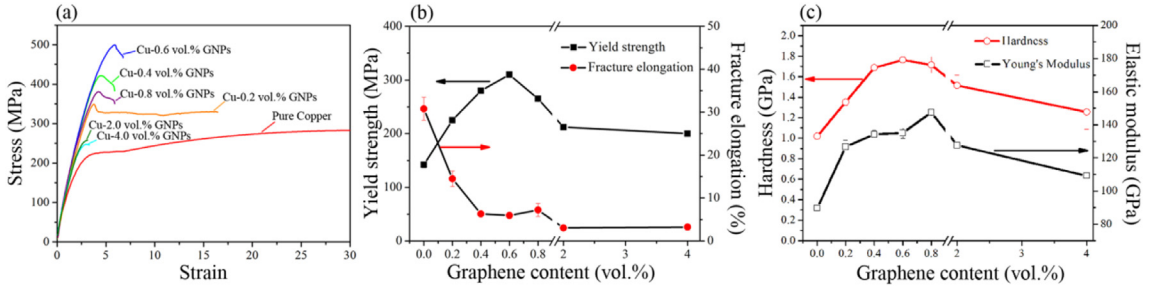

Fig. 3. (a) Stress-strain curves of Cu/GNPs composites, (b) yield strength and fracture elongation and (c) elastic modulus and hardness of Cu/GNPs composites as a function of GNPs content. (A colour version of this figure can be viewed online.)

($\alpha_{horizontal}$) to the direction of consolidation force were tested by taking one LFA sample at each corresponding direction, as illustrated in Fig. 4a. Fig. 4b demonstrates that the thermal performance of copper was evidently deteriorated by graphene addition. Both $\alpha_{vertical}$ and $\alpha_{horizontal}$ significantly decrease with the increase of graphene concentration, especially when the graphene content is over 0.8 vol.%. However, compared with copper matrix composites with other fillers, Cu/GNPs composites possess relatively good thermal conduction [26–28].

The decrease of thermal diffusivity induced by graphene addition is due to three mechanisms. Firstly, the mean-free path (MFP) of heat carrier was reduced due to the decreased matrix grain size and increased dislocation density [29]. Second, the interfacial thermal resistance was raised by the large thermal expansion mismatch and poor adherence between copper and graphene [30]. Third, voids formed during sintering served as insulating barriers to the heat flow. The inset program in Fig. 4b shows that the relative density of the composites keeps decreasing with the increase of graphene content, indicating a constant increase of voids.

By comparing $\alpha_{vertical}$ and $\alpha_{horizontal}$ of each composite, it is found that the difference between the values is varied with the graphene content. For the composites with 0.2 vol.% and 0.8 vol.% graphene, $\alpha_{horizontal}$ is almost equivalent to $\alpha_{vertical}$. However, for the composites with 2.0 vol.% and 4.0 vol.% graphene, $\alpha_{horizontal}$ is considerably larger than $\alpha_{vertical}$. This is attributed to the difference of graphene distribution in the composites. As the GNPs were distributed randomly in the composites with 0.2 vol.% 0.8 vol.% GNPs, there was no difference between the LFA samples taken from the two directions. For the composites with 2.0 vol.% and 4.0 vol.% graphene, as the GNPs aligned along the perpendicular direction of consolidation force, $\alpha_{horizontal}$ and $\alpha_{vertical}$ are the thermal diffusivity along the in-plane direction and through-plane direction of graphene, respectively. It is well known that the thermal diffusivity of graphene at the in-plane direction is thousands times larger than that at the through-plane direction, which explains the large difference of $\alpha_{horizontal}$ and $\alpha_{vertical}$. Thus, anisotropy thermal performance of Cu/GNPs was obtained by addition of high graphene content.

The electrical conductivity of the composites was also measured by eddy-current method. It decreases with increasing graphene content in Fig. 4c. Similar to the thermal performance, the constant deteriorated electrical conductivity is due to the decrease of electron MFP caused by graphene addition. However, even when the graphene content increases to 4.0 vol.%, the electrical conductivity is still more than 85% of the reference copper, which indicates that the graphene addition did not weaken the electrical conductivity of copper seriously.

3.4. Tribological performance of Cu/GNPs composites

Graphene is regarded as a novel solid lubricant as its excellent performance in previous studies [31–34]. Fig. 5 shows the influence of graphene content on the tribological performance of Cu/GNPs composites. The friction coefficient (CoF) for each kind of material varied with sliding time is summarized in Fig. 5a. The reference copper exhibited the worst anti-friction performance (CoF ≈ 0.6). Adding small amount of graphene did not improve the anti-friction property, as the CoFs of both Cu-0.2 vol.% GNPs and Cu-0.4 vol.% GNPs stay around 0.6 at the stable stage. However, the CoF reduces constantly when further increasing graphene content. The CoF of composite with 4.0 vol.% is about 0.25 which is 60% lower than reference copper. Fig. 5b shows the profiles of wear tracks at the end of wear test for reference copper and Cu/GNPs composites. Evidently, adding graphene improved the anti-wear performance of copper, especially when the graphene content was more than 0.8 vol.%.

To investigate the tribological mechanism of the materials, SEM morphologies of the worn surfaces were investigated (Fig. 6). For

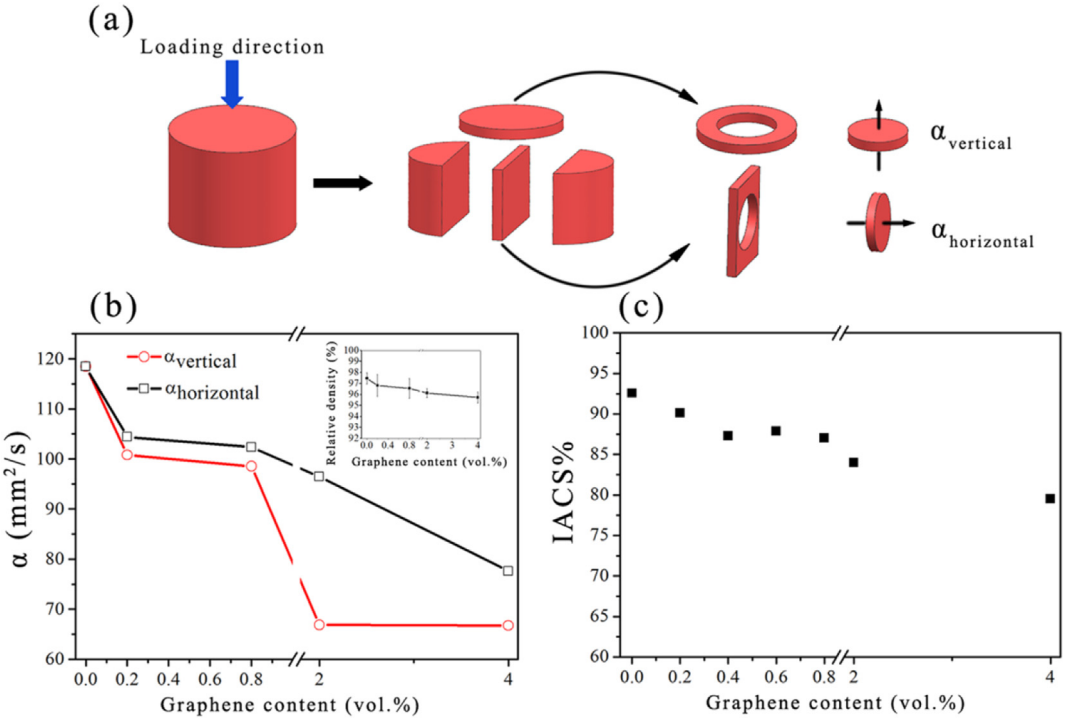

Fig. 4. (a) Sample preparation method for thermal diffusivity test, (b) thermal diffusivity and relative density (insert program) as a function of GNPs content and (c) electrical conductivity of Cu/GNPs composites. (A colour version of this figure can be viewed online.)

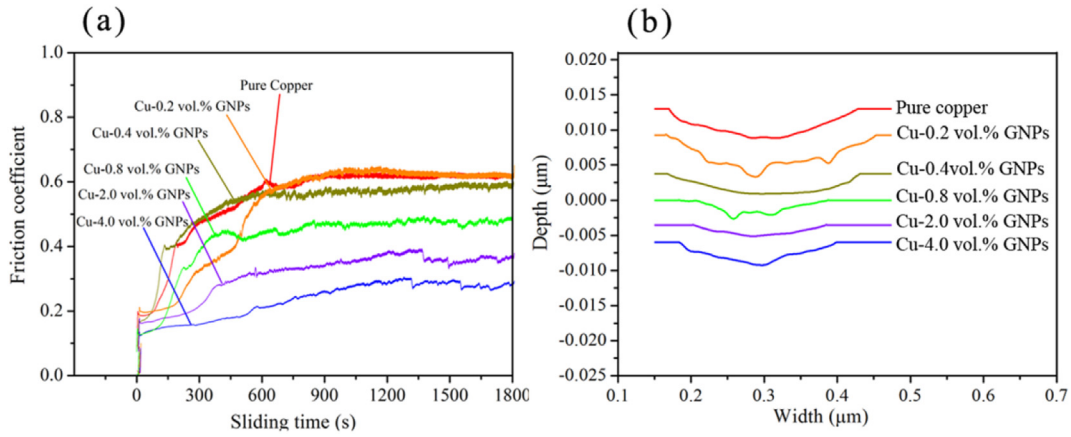

Fig. 5. (a) Friction coefficients for the Cu/GNPs composites varied with sliding time and (b) profiles of the wear tracks. (A colour version of this figure can be viewed online.)

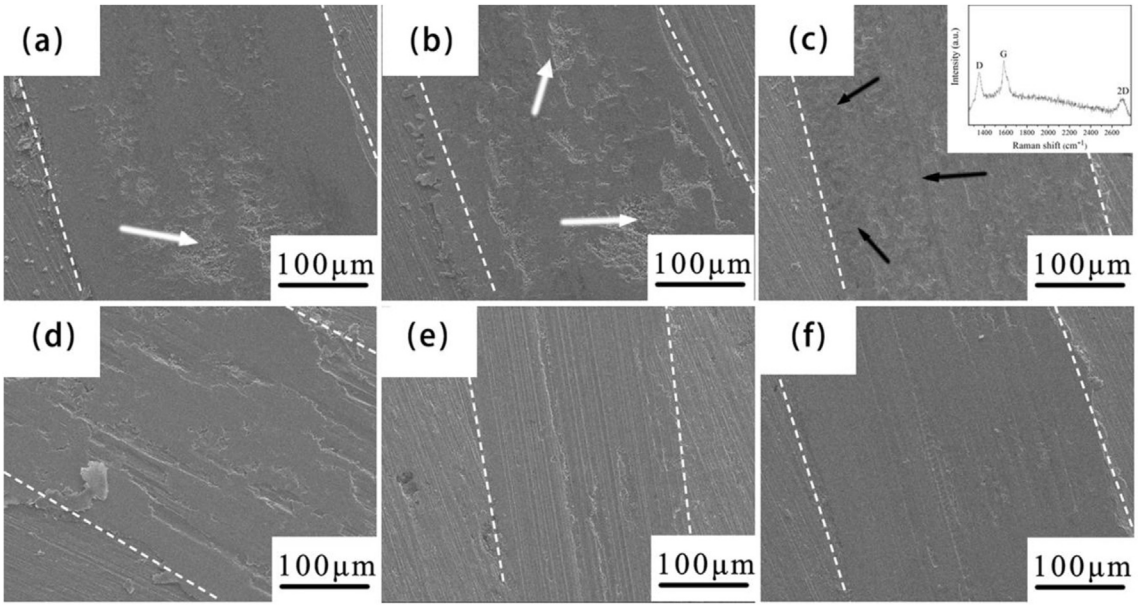

Fig. 6. SEM morphologies of the wear tracks: (a) pure copper, (b) Cu-0.2 vol.% GNPs, (c) Cu-0.4 vol.% GNPs, (d) Cu-0.8 vol.% GNPs, (e) Cu-2.0 vol.% GNPs and (f) Cu-4.0 vol.% GNPs.

reference copper, there are rupture symbols with fine debris on the worn surface, as pointed out by the white arrows in Fig. 6a. As the sliding process continued, the worn surface metal was oxidized due to the high contact temperature, indicated by the EDS results in Fig. S3 (Supporting information). The as-formed oxide inclusions restricted the movement of the dislocations generated by the plastic deformation at the interface, which caused an area with high stress and great strain at the sub-surface [35]. In the following sliding process, surface raptured occurred once local stress reached the fracture strength, leading to large wear loss. There is no big difference of the worn surfaces between Cu-0.2 vol.% GNPs and reference copper. However, when the graphene content reaches to 0.4 vol.%, the rupture feature significantly reduces and island-like dark films is observed in Fig. 6c, indicated by black arrows. By Raman analysis (insert graph in Fig. 6c), graphene was detected in the films. As the graphene content increased, GNPs were squeezed out of the composites and connected with the wear debris at the worn surface, forming well consolidated graphene rich films. The spread of the films on the contact interface not only prohibited the matrix from oxidation but also reduced friction due to the weak shearing strength of graphene. However, as the films were thin and not continuous, they were quickly worn out by friction. This explains the unobvious decrease of friction coefficient. When the graphene content further increases, the graphene rich films become continuous and got thicker in Figure d, e and f. Once an integrated graphene rich film was formed on wear track, the relative sliding between the counterparts was proceed in the films. As the shear strength of graphene film is considerably low, it reduces wear and friction effectively.

The present work demonstrates that Cu/GNPs composites had evidently strengthened mechanical and tribological performance and possessed good thermal and electrical conduction simultaneously. It suggests that Cu/GNPs composite could serve as a potential electrical contact material. However, as the graphene content had great impacts on these properties, choosing a proper graphene content to achieve comprehensive performance of composite is important. Furthermore, according to the mechanism analysis, the graphene strengthen efficiency was largely limited by

the interfacial bonding strength between graphene and copper matrix. In order to further improve the performance of Cu/GNPs composite, our future work aims to improve the interfacial bonding strength by tailoring the interfacial nanostructures.

4. Conclusions

Copper matrix composites with varied graphene contents were prepared via molecular-level mixing process and SPS process. The distribution of GNPs in matrix was influenced by its concentration. GNPs alignment was achieved in composites with graphene more than 2.0 vol.%. For mechanical performance, the composites were strengthened by graphene addition in three mechanisms: high generated dislocation density, grain refinement and load transfer effects. With the increase of graphene content, the strengthen effect was firstly enhanced and then deteriorated. Both the thermal and electrical conductivity slightly decreased when graphene content increased. Anisotropy thermal performance was obtained in composites with GNPs alignment. For tribological performance, graphene addition was beneficial for wear resistance and friction reduction. Our findings may lead to the application of copper/graphene composite in electrical contact component production.

Acknowledgments

The authors gratefully acknowledge the National Natural Science Foundation of China (91426304) and the Ningbo Municipal Key Project (2014S10001) for the financial support, Ningbo Powerway Alloy Material Co. Ltd. for electrical conductivity testing and Ningbo Morsh Technology. Co. Ltd. for free graphene supporting.

Appendix A. Supplementary data

Supplementary data related to this article can be found at http://dx.doi.org/10.1016/j.carbon.2015.10.023.

References

[1] S. Stankovich, D.A. Dikin, G.H.B. Dommett, K.M. Kohlhaas, E.J. Zimney, E.A. Stach, et al., Graphene-based composite materials, Nature 442 (7100) (2006) 282–286.

[2] X. Huang, X. Qi, F. Boey, H. Zhang, Graphene-based composites, Chem. Soc. Rev. 41 (2) (2012) 666–686.

[3] M.A. Rafiee, J. Rafiee, Z. Wang, H. Song, Z.-Z. Yu, N. Koratkar, Enhanced mechanical properties of nanocomposites at low graphene content, ACS Nano 3 (12) (2009) 3884–3890.

[4] M. Fang, K. Wang, H. Lu, Y. Yang, S. Nutt, Covalent polymer functionalization of graphene nanosheets and mechanical properties of composites, J. Mater. Chem. 19 (38) (2009) 7098–7105.

[5] T. Kuilla, S. Bhadra, D. Yao, N.H. Kim, S. Bose, J.H. Lee, Recent advances in graphene based polymer composites, Prog. Polym. Sci. 35 (11) (2010) 1350–1375.

[6] T. Wei, G. Luo, Z. Fan, C. Zheng, J. Yan, C. Yao, et al., Preparation of graphene nanosheet/polymer composites using in situ reduction-extractive dispersion, Carbon 47 (9) (2009) 2296–2299.

[7] L.-Y. Chen, H. Konishi, A. Fehrenbacher, C. Ma, J.-Q. Xu, H. Choi, et al., Novel nanoprocessing route for bulk graphene nanoplatelets reinforced metal matrix nanocomposites, Scr. Mater. 67 (1) (2012) 29–32.

[8] J. Dutkiewicz, P. Ozga, W. Maziarz, J. Pstruś, B. Kania, P. Bobrowski, et al., Microstructure and properties of bulk copper matrix composites strengthened with various kinds of graphene nanoplatelets, Mater. Sci. Eng. A 628 (0) (2015) 124–134.

[9] Z. Ren, N. Meng, K. Shehzad, Y. Xu, S. Qu, B. Yu, et al., Mechanical properties of nickel-graphene composites synthesized by electrochemical deposition, Nanotechnology 26 (6) (2015) 065706.

[10] L. Debrupa, A. Arvind, Graphene: synthesis and applications, in: C. Jo-won, L. Wonbong (Eds.), Graphene-reinforced Ceramic and Metal Matrix Composites, Taylor and Francis Publishers, 2011, pp. 187–232.

[11] N. Darsono, D.-H. Yoon, J. Kim, Milling and dispersion of multi-walled carbon nanotubes in texanol, Appl. Surf. Sci. 254 (11) (2008) 3412–3419.

[12] K. Morsi, A. Esawi, Effect of mechanical alloying time and carbon nanotube (CNT) content on the evolution of aluminum (Al)–CNT composite powders, J. Mater. Sci. 42 (13) (2007) 4954–4959.

[13] J. Hwang, T. Yoon, S.H. Jin, J. Lee, T.-S. Kim, S.H. Hong, et al., Enhanced mechanical properties of graphene/copper nanocomposites using a molecular-level mixing process, Adv. Mater. 25 (46) (2013) 6724–6729.

[14] M. Li, H. Che, X. Liu, S. Liang, H. Xie, Highly enhanced mechanical properties in Cu matrix composites reinforced with graphene decorated metallic nanoparticles, J. Mater. Sci. 49 (10) (2014) 3725–3731.

[15] C.L.P. Pavithra, B.V. Sarada, K.V. Rajulapati, T.N. Rao, G. Sundararajan, A new electrochemical approach for the synthesis of copper-graphene nanocomposite foils with high hardness, Sci. Rep. 4 (2014) 4049.

[16] W.J. Kim, T.J. Lee, S.H. Han, Multi-layer graphene/copper composites: preparation using high-ratio differential speed rolling, microstructure and mechanical properties, Carbon 69 (2014) 55–65.

[17] Y. Kim, J. Lee, M.S. Yeom, J.W. Shin, H. Kim, Y. Cui, et al., Strengthening effect of single-atomic-layer graphene in metal-graphene nanolayered composites, Nat. Commun. 4 (2013).

[18] K. Chu, C. Jia, Enhanced strength in bulk graphene-copper composites, Phys. Status Solidi A 211 (1) (2014) 184–190.

[19] A.C. Ferrari, J.C. Meyer, V. Scardaci, C. Casiraghi, M. Lazzeri, F. Mauri, et al., Raman spectrum of graphene and graphene layers, Phys. Rev. Lett. 97 (18) (2006) 187401.

[20] D. Yoon, H. Moon, H. Cheong, J.S. Choi, J.A. Choi, B.H. Park, Variations in the Raman spectrum as a function of the number of graphene layers, J. Korean Phys. Soc. 55 (3) (2009) 1299–1303.

[21] A. Boden, B. Boerner, P. Kusch, I. Firkowska, S. Reich, Nanoplatelet size to control the alignment and thermal conductivity in copper-graphite composites, Nano Lett. 14 (6) (2014) 3640–3644.

[22] J.N. Wei, Z.B. Li, F.S. Han, Thermal mismatch dislocations in macroscopic graphite particle-reinforced metal matrix composites studied by internal friction, Phys. Status Solidi A 191 (1) (2002) 125–136.

[23] K.T. Kim, S. Il Cha, T. Gemming, J. Eckert, S.H. Hong, The role of interfacial oxygen atoms in the enhanced mechanical properties of carbon-nanotube-reinforced metal matrix nanocomposites, Small 4 (11) (2008) 1936–1940.

[24] Z. Zhang, D.L. Chen, Consideration of Orowan strengthening effect in particulate-reinforced metal matrix nanocomposites: a model for predicting their yield strength, Scr. Mater. 54 (7) (2006) 1321–1326.

[25] Y. Wu, E.J. Lavernia, Strengthening behavior of particulate reinforced MMCs, Scr. Metall. 27 (2) (1992) 173–178.

[26] J. Li, H. Zhang, Y. Zhang, Z. Che, X. Wang, Microstructure and thermal conductivity of Cu/diamond composites with Ti-coated diamond particles produced by gas pressure infiltration, J. Alloy Compd. 647 (2015) 941–946.

[27] W. Yang, L. Zhou, K. Peng, J. Zhu, L. Wan, Effect of tungsten addition on thermal conductivity of graphite/copper composites, Compos. Part B Eng. 55 (2013) 1–4.

[28] J. Kováčik, Š. Emmer, J. Bielek, Thermal conductivity of Cu-graphite composites, Int. J. Therm. Sci. 90 (2015) 298–302.

[29] P. Goli, H. Ning, X. Li, C.Y. Lu, K.S. Novoselov, A.A. Balandin, Thermal properties of graphene–copper–graphene heterogeneous films, Nano Lett. 14 (3) (2014) 1497–1503.

[30] C.W. Nan, R. Birringer, D.R. Clarke, H. Gleiter, Effective thermal conductivity of particulate composites with interfacial thermal resistance, J. Appl. Phys. 81 (10) (1997) 6692–6699.

[31] C.F. Gutierrez-Gonzalez, A. Smirnov, A. Centeno, A. Fernandez, B. Alonso, V.G. Rocha, et al., Wear behavior of graphene/alumina composite, Ceram. Int. 41 (6) (2015) 7434–7438.

[32] W. Zhai, X. Shi, M. Wang, Z. Xu, J. Yao, S. Song, et al., Grain refinement: a mechanism for graphene nanoplatelets to reduce friction and wear of Ni3Al matrix self-lubricating composites, Wear 310 (1–2) (2014) 33–40.

[33] D. Berman, A. Erdemir, A.V. Sumant, Graphene: a new emerging lubricant, Mater. Today 17 (1) (2014) 31–42.

[34] J. Lin, L. Wang, G. Chen, Modification of graphene platelets and their tribological properties as a lubricant additive, Tribol. Lett. 41 (1) (2011) 209–215.

[35] Y.H. Qiang, S.R. Ge, Q.J. Xue, Microstructure and tribological behaviour of nitrocarburizing-quenching duplex treated steel, Tribol. Int. 32 (3) (1999) 131–136.